01 Jun 2014

Fabrication of Multifunctional Ferromagnetic Au_3Pd-CoSe Nanoparticles

Wipula P. Liyanage

Sukhada Mishra

Kai Song

Manashi Nath
Missouri University of Science and Technology, nathm@mst.edu

Recommended Citation

W. P. Liyanage et al., "Fabrication of Multifunctional Ferromagnetic Au_3Pd-CoSe Nanoparticles," *RSC Advances*, vol. 4, no. 53, pp. 28140-28147, Royal Society of Chemistry, Jun 2014.
The definitive version is available at https://doi.org/10.1039/c4ra02264e

RSC Advances

PAPER

View Article Online
View Journal | View Issue

Fabrication of multifunctional ferromagnetic Au_3Pd–CoSe nanoparticles†

Cite this: *RSC Adv.*, 2014, **4**, 28140

Wipula P. R. Liyanage,‡[a] Sukhada Mishra,‡[a] Kai Song§[b] and Manashi Nath*[a]

Received 14th March 2014
Accepted 12th June 2014

DOI: 10.1039/c4ra02264e

www.rsc.org/advances

We have synthesized multifunctional anisotropic Au_3Pd–CoSe nanoparticles on Si substrate through a catalyst aided chemical vapour deposition technique. The technique utilized volatile cobalt acetylacetonate and elemental selenium as precursors while sputter coated Au–Pd (3 : 2) film acted as a catalyst. The typical growth conditions led to clear segregation of the hetero-compositions (*i.e.* Au_3Pd and CoSe) in the product nanostructures thereby preserving the functionality of both the phases. The degree of crystallinity of the individual phases in the composite nanostructure was fairly high. The bifunctional nanoparticles show soft ferromagnetic behaviour at room temperature and optical activity making them ideal for opto-magnetic applications.

Introduction

Multifunctional nanostructures are explored extensively for their various applications including those in biosciences such as molecular imaging, magnetic separation, fluorescent labelling and other *theranostic* uses.[1,2] The capability to tune the size, shape and morphology in addition to the composition of these multifunctional nanomaterials provides them with even more versatility. Multifunctional nanomaterials can be categorized according to their morphologies as core–shell (where heterocomposition is expressed radially),[3] dumbbell shaped (where heterocompositions are segregated along the long axis of the nanostructure)[4] and barcode structures.[5] The functionalities of the individual regions can be varied to obtain various types of multifunctional nanomaterials. The dumbbell shaped nanoparticles containing two compositions of widely different functionalities sharing a common interface is especially lucrative since it provides opportunities to fully utilize both the functionalities in the nanoparticle ensemble. These types of multifunctional particles are also referred to as *Janus* particles when they are more spherical than elongated.[6] Amongst these, nanostructures including a metallic and a magnetic composition have been of considerable interest due to their promising applications in magneto-optic and optoelectronic devices. Development in the field of nanotechnology has also contributed to the advancement of practical applications of the multifunctional nanoparticles in nanomedicine as *theranostic* agents.[7] Owing to its, biocompatibility and localized surface plasmon resonance (SPR) properties, Au nanoparticles have been very well analysed component of the multifunctional nanoparticle assemblies.[7,8] The optical properties of the Au imparts major advantages, as the SPR peak of the Au nanoparticles can be adjusted to near-infrared region, by tuning the size of the nanoparticles where the biological tissues being 'nearly transparent' at these wavelengths, do not absorb in these regions thus reducing background noise. Accordingly, various multifunctional nanoparticles containing Au, such as Au–Fe_2O_3, Au–FePt, Au–Fe_3O_4 has been synthesized by different techniques involving solution-based chemistry.[8–10]

The transition metal chalcogenides (ME_x) [M = Fe, Co, Mn; E = Se, S, Te] have attracted the solid state chemists for a long time owing to their interesting electronic and magnetic properties.[11] Among them, CoSe is a semiconducting material with the band gap of 1.52 eV. Cobalt selenides typically show compositions ranging from the stoichiometric CoSe, $CoSe_2$ phases to the non-stoichiometric $Co_{0.85}Se$ phase.[12–15] Cobalt selenide is known to be a metallic conductor and exchange-enhanced Pauli paramagnet in its ground state with a T_c of approximately 125 K.[12–15] Recently cobalt selenides have shown lot of promise as catalysts for oxygen reduction, decomposition of hydrazine hydrate, magnetic refrigeration and as electrodes for Li-ion batteries.[16] CoSe in bulk form has been synthesized through electrochemical deposition technique,[17] high pressure solid-state synthesis[18] and through mechanical alloying.[19] However, reports of cobalt selenide nanostructures are very limited.[20–22] CoSe nanoparticles have been synthesized through microwave assisted methods[20] while CoSe nanocrystals were

[a]*Department of Chemistry, Missouri University of Science and Technology, 400 W 11th Street, Rolla, MO 65409, USA. E-mail: nathm@mst.edu; Fax: +1 (573)341-6033; Tel: +1 (573)341-7160*

[b]*Materials Research Centre, Missouri University of Science and Technology, Rolla, MO 65409, USA*

† Electronic supplementary information (ESI) available: Magnetization *vs.* temperature for blank Si substrate and XPS spectra of the nanoparticles. See DOI: 10.1039/c4ra02264e

‡ These authors contributed equally to this conducted research.

§ Current address: FEI Company, 5350 NE Dawson Creek Drive, Hillsboro, Oregon 97124, USA; Tel: +1 (860)768-8121.

also formed using metal acetate–paraffin approach, in the presence of oleylamine,[21] and by hydrothermal method in presence of hydrazine, cobalt chloride and selenium.[22]

In this article, we report the synthesis, characterization and properties of Au_3Pd–CoSe bifunctional nanoparticles, which show magnetic ordering as well as optical activity. These nanoparticles have been produced by a simple chemical vapour deposition (CVD) reaction and are the first of its kind. The bifunctional nature of these composite nanoparticles was characterized through optical and magnetic properties. The fusion of optical and magnetic properties in these nanoparticles will be useful for applications in various fields like opto-magnetic devices, biomedical and bioimaging platforms.

Experimental

Materials & methods

Si substrates used for chemical vapour deposition were purchased from Si quest international. These Si substrates were cut into pieces of 1×1 cm^2 and prewashed with isopropanol and acetone in order to remove dirt particles. No extra precautionary step was taken to remove the native oxide layer. The substrates were then sputter coated with Au–Pd (3 : 2) for 120 seconds creating a thick layer (approximately 100 nm) of Au–Pd over the substrates. Cobalt acetylacetonate [$Co(C_5H_7O_2)_3$, $Co(acac)_3$] and Se shots, used as precursors for Co and Se, respectively were obtained from Sigma-Aldrich and used as such, without further purification.

Synthesis of Au_3Pd–CoSe composite nanoparticles

Au_3Pd–CoSe nanoparticles were synthesized by catalyst aided CVD reaction carried out in a horizontal tube furnace at 800 °C under a flow of N_2 as carrier gas (120 sccm). A Au–Pd (3 : 2) coated Si wafer used as the substrate for growth was kept at the central region of the horizontal furnace at 800 °C. With the help of a mass flow controller the reaction assembly was maintained at a continuous N_2 flow of 120 sccm. Both the $Co(acac)_3$ and Se sublime at elevated temperatures and hence they were strategically placed within the reaction tube such that the temperature at the precursors just exceeded their sublimation temperature when the central zone of the furnace was at 800 °C. Selenium shots were positioned at 400 °C, while the $Co(acac)_3$ was kept at a 250 °C region. Initially, the $Co(acac)_3$ and Se were kept outside the heating zone by pushing the ceramic liner to the extreme left. Once the central zone of the furnace reached the reaction temperature (800 °C), the ceramic liner was pushed to the right such that the Se and $Co(acac)_3$ were at 400 °C and 250 °C respectively. These steps were crucial for reproducibility of the reaction, as it avoids the sublimation and escape of the reactants (Se and $Co(acac)_3$ vapors) before the Au/Pd catalyst reaches the melting temperature. The reaction was carried out for 30 minutes, and the furnace was cooled down at the rate of 8 °C min^{-1}. After completion of the reaction a golden brown deposition was observed on the Si substrate. This deposition was further characterized for elucidation of the morphology and composition of the product.

Characterization tools & techniques

Powder X-ray diffraction. The product was characterized without any subsequent purification through powder X-ray diffraction (pxrd) with Philips X-Pert using CuKα (1.5418 $\propto$) radiation. Pxrd pattern was collected from the as-synthesized product spread on the Si substrate. Because the product formed a very thin layer on the Si substrate, the pxrd was collected at grazing angles in thin film geometry (GI mode with Göbel mirrors).

Electron microscopy characterizations

For transmission electron microscopy (TEM) imaging, the sample was prepared by loosening a small amount of product from the Si substrate (typically, the deposition on Si substrate was scratched) and dispersing it in ethanol. A drop from the "as prepared" dispersion was placed a holey carbon coated Cu TEM grid and dried in air thoroughly prior to TEM imaging and Energy dispersive X-ray spectroscopy (EDS). TEM images were obtained on FEI Tecnai F20 and Tecnai Osiris TEM operating at 200 kV. For FEI Tecnai Osiris TEM the probe current is 1 nA with a spot size of less than 1 nm. The convergence angle is 10.3 mrad and the camera length is 200 mm for HAADF imaging. High resolution TEM in Fig. 3 was obtained with the Tecnai Osiris operated at 200 keV with a probe current of 2.5 nA. The Fast Fourier Transform (FFT) patterns generated from the lattice fringes clearly demonstrated the crystalline character of the individual regions, *i.e.* Au_3Pd and CoSe.

Scanning electron microscope (SEM) imaging was performed using FEI Helios NanoLab 600 FIB/FESEM directly onto the Si substrate covered with the nanoparticles. SEM and EDS imaging was also performed by isolating a small amount of powder from the Si substrate and putting it on the sample holder. The EDS line scan and mapping as shown in Fig. 2 was conducted on an FEI Tecnai F20 TEM operated at 200 keV in STEM mode. The probe current is 1.2 nA with a spot size of less than 2 nm. The convergence angle is 13 mrad and the camera length is 30 mm for dark field imaging. This scope is equipped with an Oxford ultra-thin (UTW) window EDS detector, which allows detection of carbon. The X-ray transmission efficiency for carbon with this window is 42%.

Magnetic characterizations

A magnetic moment was collected from a SQUID magnetometer in the VSM mode. The Si-substrate containing large density of Au_3Pd–CoSe composite nanoparticles was loaded into a gel cap and was inserted into the magnetometer with the help of standard sample loader. The diamagnetic signal from the gel cap was collected separately and subtracted as a background from the signal obtained from the sample. The zero field cooled (ZFC) data was obtained after cooling the sample down to ~2 K under 0 magnetic fields and then by measuring the magnetization under an applied field during the warming up cycle. The field cooled warming (FCW) data was collected by cooling the sample down from room temperature to 2 K under a non-zero magnetic field and then collecting the warming up data under

an applied field. The magnetization of a blank Si substrate which was heat treated under similar conditions was also collected separately and used as a reference.

Optical characterizations

Varian Cary 50 UV-Vis Spectrophotometer was used for optical property measurements. Sample preparation for the UV-Vis spectroscopy involved two separate methods. In one method the composite nanoparticles were dislodged from the Si substrate and sonicated in ethanol for about 30 minutes. This dispersion was then loaded in a quartz cuvette and the absorbance spectra were recorded while the nanoparticles were still dispersed. The second method involved functionalization of these bifunctional nanoparticles through the affinity of Au with thiol-based ligands. Typically the Au_3Pd–CoSe nanoparticles were dislodged from the Si substrate and added to an ethanolic solution of 1-octadecanthiol forming a stable dispersion. This dispersion was then dried on top of glass slides which were then loaded in the sample chamber of the UV-Vis spectrometer.

Results & discussion

Morphology, composition and structural characterization

Fig. 1a demonstrates the pxrd pattern obtained from the product, confirming the presence of hexagonal CoSe (JCPDS card no. 42541) and Au_3Pd (JCPDS no. 180872) formed from the catalyst. The intense and sharp pxrd peaks suggest highly crystalline nature of the formed product. Noticeably, the product purity was very high and it did not exhibit presence of any crystalline impurity from other cobalt selenide phases. Fig. 1b shows the SEM image of the product, revealing a huge yield of the elliptical-shaped nanoparticle morphology. The shape and nature of these nanoparticles are very representative of the bifunctional *Janus* particles.[6] The presence of hetero-composition zones in the nanoparticle was very apparent as can be seen from the different contrasts in the SEM images. The composite nanoparticles were mostly elliptical in shape with the short axis ranging from 100–150 nm while the catalyst tip was less than 100 nm. The nanoparticle size distribution was

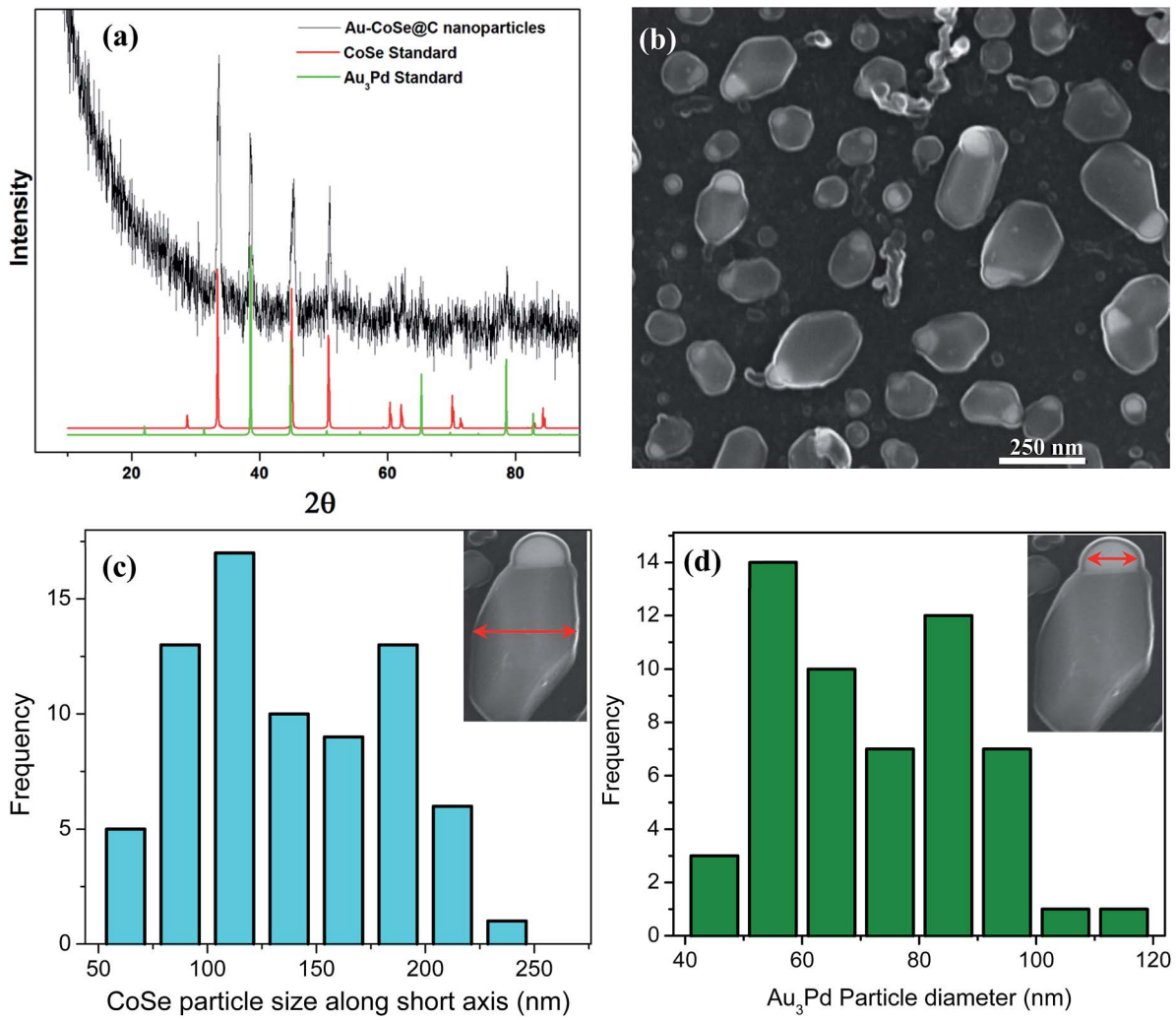

Fig. 1 (a) PXRD pattern of the Au_3Pd–CoSe nanoparticles showing presence of CoSe along with Au_3Pd. (b) SEM image of the bifunctional nanoparticles. Brighter tip represents Au_3Pd, while darker region contains CoSe. (c) Particle size distribution (along short axis) of Au_3Pd–CoSe nanoparticles. (d) Particle size distribution (*i.e.* diameter) of the Au–Pd region.

estimated by analyzing large number of these nanoparticles and the corresponding histogram is shown in Fig. 1c (corresponding to the short axis of the elliptical particles) and 1d (corresponding to the catalyst tip/cap). Histogram analysis also showed that the particle sizes (along the long axis) were mostly in the range 200–250 nm. In almost all the nanoparticles, heterozones were observed longitudinally while radial heterojunctions (core–shell) were not present. The size of these composite nanoparticles could be somewhat controlled by changing the size of the initial Au–Pd nanoalloy catalyst particles.

The elemental compositions of these bifunctional nanoparticles were investigated in details through extensive elemental analysis studies including EDS line scan and mapping in STEM mode. The elemental mapping from these individual nanoparticles showed that Co and Se were concentrated at the thicker end of the nanoparticle while Au and Pd was immobilized at the slender tip as shown in Fig. 2. The Au(Pd) and Co–Se regions shared a common interface. There was no noticeable mixing of Au in the Co–Se regions, and likewise there was almost no mixing of Co–Se in the Au region. This indicates that the phase purity of the individual phases in these bifunctional nanoparticles was very high. Although pxrd showed that the metallic part was mainly formed by Au_3Pd, there is a possibility that trace amounts of Au was also present. Au and Pd forms Au_3Pd alloy in a narrow temperature range.[23] The composition of these nanoparticles was also confirmed through X-ray photoelectron spectroscopy (XPS) which showed the presence of peaks corresponding to Co (2p) [778 eV] and Se (3d) [54 eV] in addition to Au (4f) and Pd (4d) as shown in Fig. S1 in ESI.† These values agree well with the reported values for CoSe.[24]

These composite nanoparticles were studied through detailed high-resolution TEM microscopy (HRTEM) to get a better insight into the composition of individual regions of the bifunctional particles as well as nature of the interface between these. These HRTEM studies showed that the thicker portion was actually crystalline CoSe phase with lattice fringes corresponding to the [100] planes, while the darker region showed mostly the presence of crystalline Au_3Pd (Fig. 3a and b). SAED pattern could also be collected from the CoSe region, which showed diffraction spots corresponding to (010), $(\bar{1}01)$ and $(\bar{1}11)$ lattice planes while the zone axis was along the $\langle 111 \rangle$ direction. HRTEM images collected near the interface revealed that the junction between CoSe and Au(Pd) phases were very clean and sharply defined (Fig. 4a and b). There was minimal mixing at the interface and there was no loss of crystalline order across the interface. The nature of the interface is very crucial since in these magnetic nanostructures pinning of magnetic flux at the interface by another magnetic material may lead to exchange bias interactions. However, in this case, the interface was very clean indicating that there was no major magnetic phase other than CoSe present in the interface.

Optical properties

Au nanostructures are well-known for their plasmonic property which gives a characteristic peak in the UV-Vis spectra.[25] It has been reported by other researchers that formation of Au_3Pd nanoparticles also shows surface plasmon bands similar to Au.[26,27] Hence UV-Vis absorbance spectra and magnetization

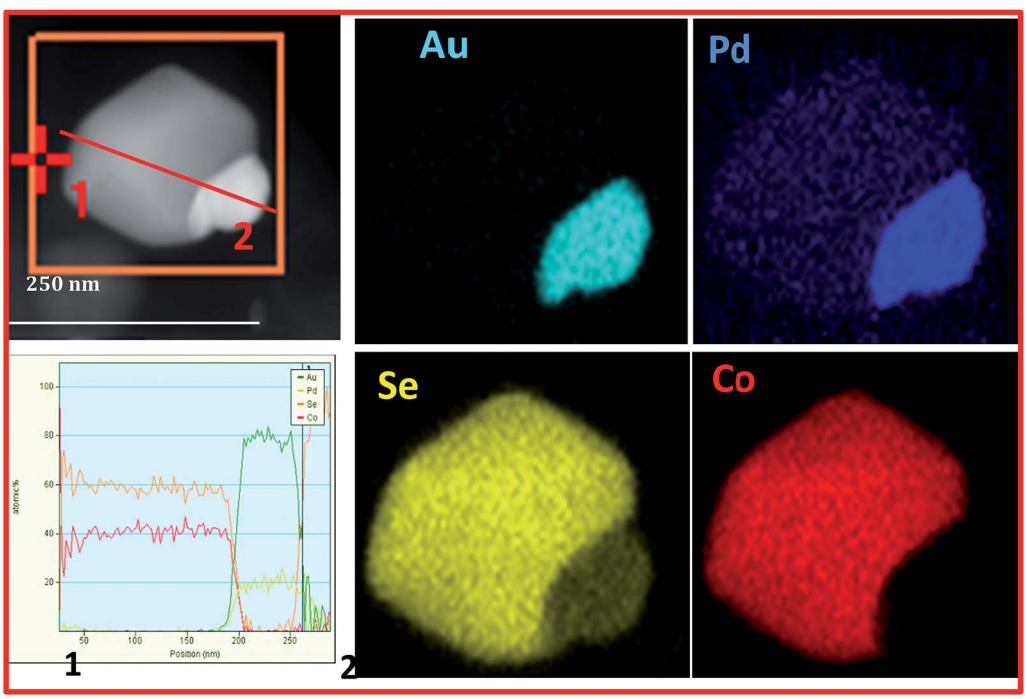

Fig. 2 Elemental mapping of the Au–CoSe nanoparticles as shown in upper left panel. Preferential location and segregation of the Au, Pd, Co and Se are shown in the mapping images. The lower left panel shows elemental line scan across the same nanoparticle which corroborates with mapping.

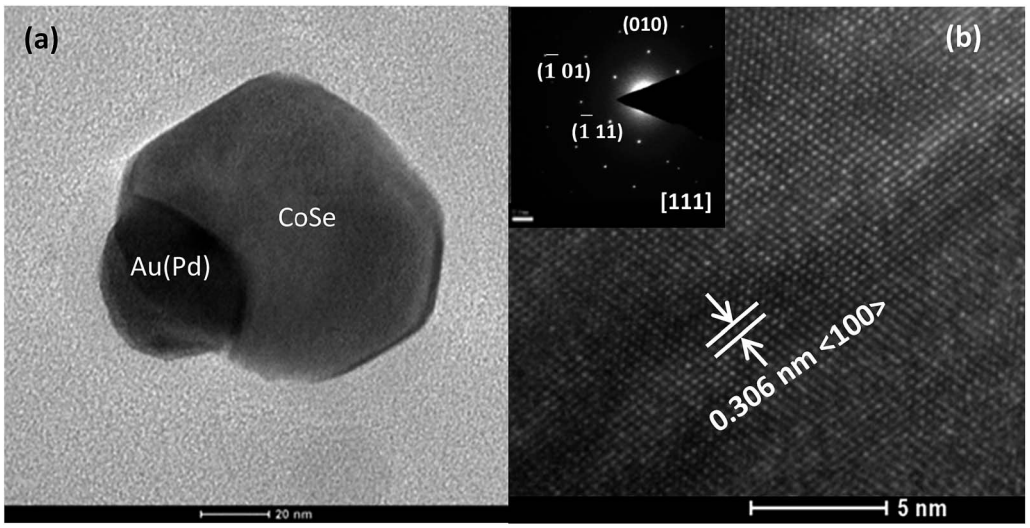

Fig. 3 (a) Magnified view of the single nanoparticle, clearly showing the union of the two nanoparticles, through a common interface. (b) HRTEM image of the CoSe region showing the lattice fringes which could be matched with ⟨100⟩ lattice planes of CoSe phase. Inset showing the SAED pattern depicting high degree of crystallinity.

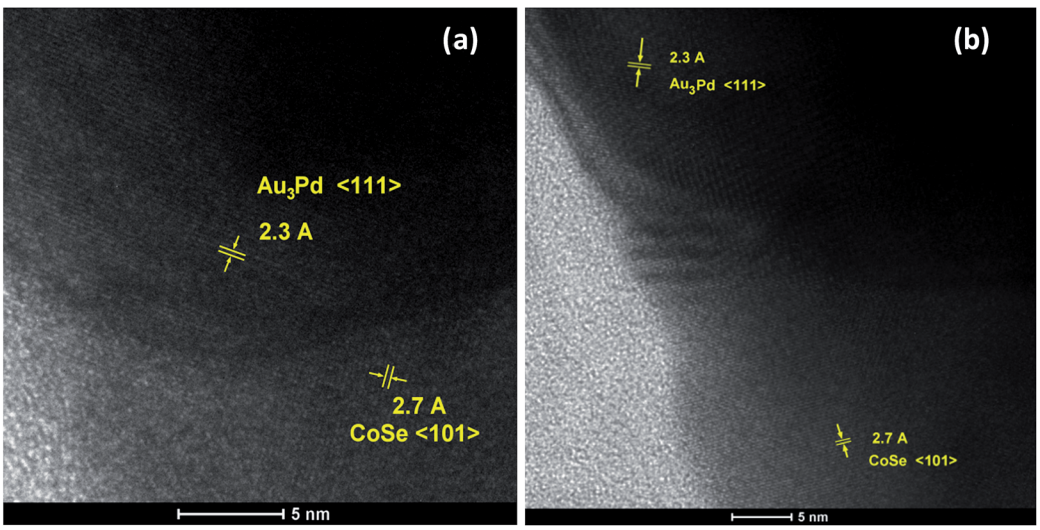

Fig. 4 (a) and (b) HRTEM images of a single nanoparticles showing clean interfaces and exhibiting lattice fringes corresponding to Au_3Pd and CoSe on either sides.

was collected from an ensemble of these Au_3Pd–CoSe nanoparticles to study their opto-magnetic properties respectively. The UV-Vis spectra of Au_3Pd–CoSe nanoparticle ensemble show a peak around 565 nm which is characteristic of Au nanostructure with a size of ~90 nm (Fig. 5a). The UV-Vis spectra also show a peak at 735 nm with a band-edge at ~750 nm corresponding to band gap energy of around 1.64 eV. This corresponds to the electronic excitation in the CoSe region, where bulk CoSe is reported to have a band-gap of 1.55 eV.[12–15] It should be noted that the plasmonic property of Au is not dampened in these composite nanoparticles. The absorbance spectrum was also collected by dispersing the Au_3Pd–CoSe nanoparticles in solution in the presence of octadecanethiol which gave a stable dispersion. This dispersion was then dried on a glass slide to form a uniform film-like deposition. This slide was then subjected to UV-Vis spectroscopy and yielded a clean spectrum with peaks at 560 nm and 750 nm similar to the ones obtained in the ethanol (Fig. 5b). It should be noted here that the octadecanethiol by itself does not show any well-defined feature in the 400–850 nm range of wavelength. Hence, the absorbance peaks obtained from the sample slide can be ascribed solely due to the Au_3Pd–CoSe nanoparticles.

Magnetic property measurement

While Au is the optically active component in these nanostructures, CoSe on the other hand is a magnetic solid which shows Pauli paramagnetism.[12–15] Magnetic property of the

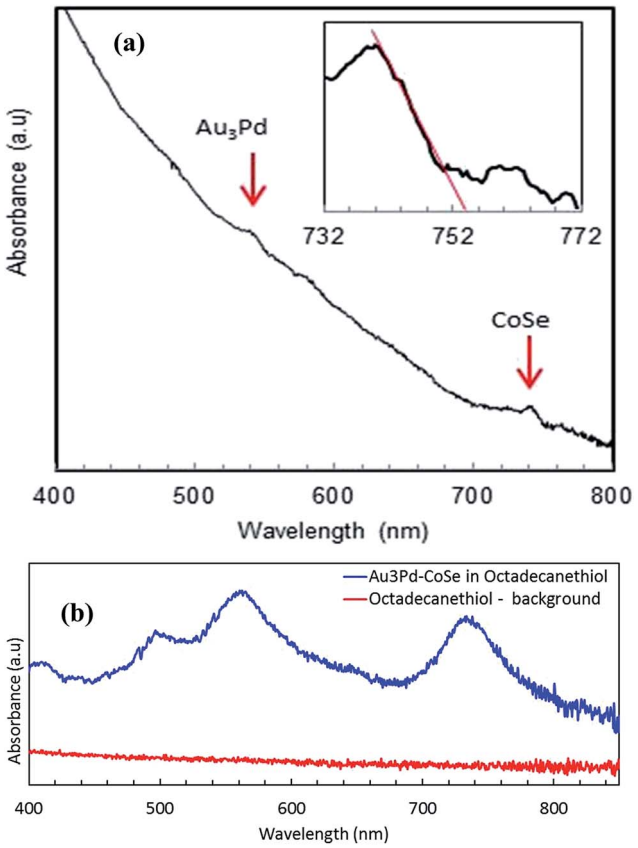

Fig. 5 Absorbance spectra obtained from Au_3Pd–CoSe bifunctional nanoparticles in (a) ethanol and (b) as a film spread on glass slide.

composite nanoparticles was studied through temperature dependent magnetization and isothermal magnetization as a function of applied field. The magnetization as a function of temperature was collected both at zero-field (ZFC) and field cooled (FC) conditions. Both ZFC and FC plot shows characteristic of a ferromagnet-like interaction at low temperatures (<10 K) (Fig. 6a). However, the data was a little bit noisy probably due to the composite nature of these nanoparticles and also the presence Si (from the substrate) in the ensemble used for magnetic measurement. The magnetic signal from Si was also collected as background, which showed featureless *M vs. T* plot as would be expected (Fig. S2†). The isothermal magnetization *vs.* field for the composite nanoparticles was collected at 300 K and 5 K (Fig. 6b). The hysteresis plots were consistent with soft ferromagnetic behavior of the composite nanoparticles. At 300 K the hysteresis loop showed a very small coercive field of ~40 Oe (Fig. 6b, right insert). At low temperatures (5 K) a clear hysteresis was also observed (Fig. 6b, left insert). However, there was a marked absence of coercivity and the magnetization had a cross-over near 0 Oe. This kind of behavior has been observed in single molecule magnets and mesoscopic granular ferromagnetic particles.[28,29] It is explained mainly by the occurrence of magnetic relaxation by quantum tunneling at low temperatures near zero fields. These kinds of magnetic relaxation are very dependent on the particle size and anisotropy. Also the presence of surface spin states causes anomalous behavior in the low temperature hysteresis loops of the nanosized magnetic particles. Hence, we suspect that the polydispersity of the CoSe regions along with varying degree of anisotropy between particles and the presence of interface with Au_3Pd give rise to competing magnetic interactions, especially at low temperatures, contributing to the complex nature of the hysteresis curve. However, the nature of the hysteresis loops indicates that the nanoparticles have considerable ferromagnetic interactions within the ensemble. The very low value of the coercive field also suggests superparamagnetic behavior, which is expected for ferromagnetic nanoparticles with sizes below the critical limit for forming monodomain magnetic particles. It was also observed that the Au_3Pd–CoSe nanoparticle ensemble was weakly attracted to a common laboratory magnet and could be magnetically separated over several days. Hence it can be

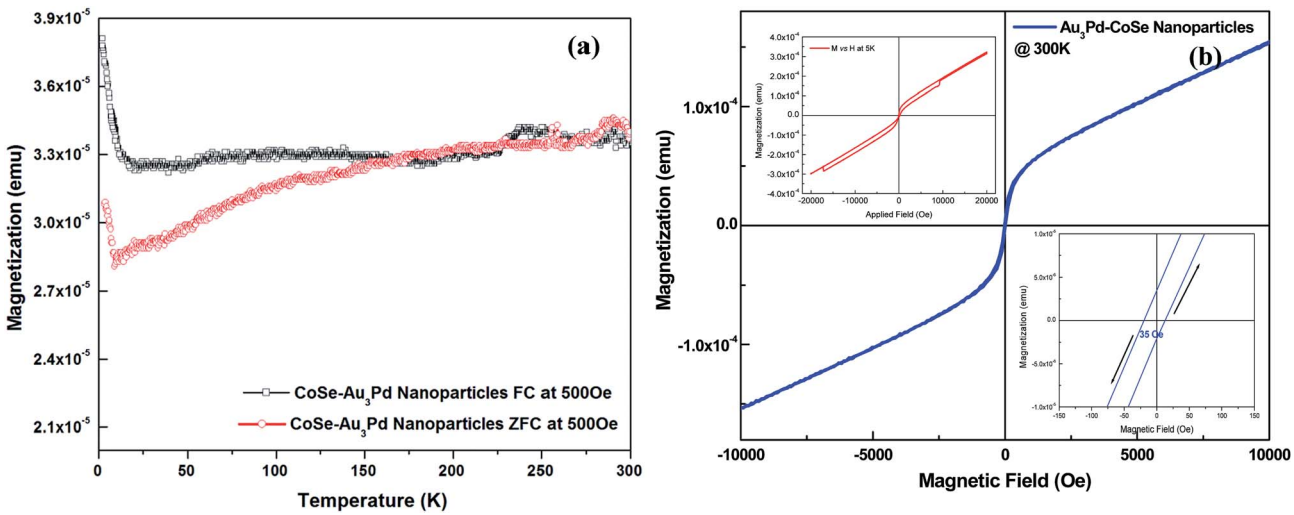

Fig. 6 The magnetization behaviour of Au_3Pd–CoSe nanoparticles. (a) *M vs. T* plot of the nanoparticles under zero-field cooled and field-cooled conditions. (b) Isothermal *M vs. H* at 300 K. Lower right inset shows the zoomed in view showing the small coercivity. Upper left inset shows the *M vs. H* plot at 5 K.

concluded that the Au_3Pd–CoSe nanoparticles have soft ferromagnetic interactions within the ensemble with low coercivity which makes them weakly responsive to external magnetic fields. Their diminishing hysteresis loop and nature of the ZFC–FC curves indicate that at 300 K they might be very near to the superparamagnetic blocking temperature separating the ordered state with the superparamagnetic state.

It was observed that the Au_3Pd–CoSe nanoparticles could be stabilized in solution by adding a thiol-based ligand (*e.g.* octadecanethiol) which shows affinity towards Au_3Pd-region. The dispersion formed by Au_3Pd–CoSe nanoparticles in ethanol in the presence of octadecanethiol was stable for several days. Interestingly, placing a magnet near the dispersion led to the very slow accumulation of Au_3Pd–CoSe nanoparticles near the magnet. This indicates that these nanoparticles reported here can be functionalized with appropriate head groups and will be ideal for application which requires multifunctional opto-magnetic components, where the magnetic part can be utilized for targeting and tracking, while the optical part aids in identification. Currently, the authors are trying to functionalize these nanoparticles with some peptide aptamers and use them for *in vitro* studies related to *theranostic* applications.

Mechanism of formation

To elucidate the growth mechanism, the authors performed several experiments by varying the reaction parameters. It was realized that the first step in this reaction scheme was the formation of Au_3Pd alloy which is the stable phase in the Au–Pd binary phase diagram within the Pd rich zone.[23] This Au_3Pd then acts as the catalysts for further decomposition and growth of the Co-rich phases. The next stage in the nanostructure growth comprises of vaporization and transport of $Co(acac)_3$ and Se. The $Co(acac)_3$ pyrolyzes under the reaction condition and the Co-rich vapours generated dissolve and diffuses preferentially within the Au_3Pd region of the catalyst. As Se vapours are fed into the system, the Co end of the catalyst gets converted into CoSe which precipitates out from one end of the active catalyst region (Au_3Pd). The limited solubility of Co and Se in Au_3Pd, facilitates the anisotropic precipitation of the CoSe phase. It should be noted here that in the composite nanoparticle there was no evidence of elemental Co and the formation reaction of CoSe was complete.

The method for nanostructure growth reported here is similar to the growth of superconducting FeSe nanocables and entrapped nanoparticles by the current authors.[30,31] In the case of FeSe nanostructures, however, the entire FeSe was encapsulated within a carbon nanofiber and carbonaceous shell, respectively, and the growing FeSe shared an interface with $Pd_{17}Se_{15}$, while Au did not take part in the reaction at all. There was no evidence of Au_3Pd formation in the case of FeSe. In the current case, however, the marked difference between the phase diagrams of Fe–Pd and Co–Pd results in completely different composition-zones in the nanostructures, *viz.* Au_3Pd alloy formation.

Conclusions

We have successfully synthesized, anisotropic, bifunctional Au_3Pd–CoSe nanoparticles, through facile, catalyst aided, chemical vapour deposition technique. The magnetic characterization of these bi-functional nanoparticles revealed their soft ferromagnetic nature. Optical activity of these nanoparticles was confirmed through observation of the plasmonic bands for Au and the absorbance peak corresponding to CoSe. The method described in this report can be used to synthesize new multifunctional nanostructures by carefully choosing various other metal-acetylacetonate precursors, and catalyst particles to synthesize metal selenide-noble metal multifunctional nanostructures.

Acknowledgements

The authors would like to acknowledge Materials Research Center for equipment usage, Dr. Kartik Ghosh, Dr. Jakub Koza and Dr. Jay Switzer for help with some magnetic measurements.

Notes and references

1 H. Zeng and S. Sun, *Adv. Funct. Mater.*, 2008, **18**, 391.
2 C. V. Durgadas, C. P. Sharma and K. Sreenivasan, *Nanoscale*, 2011, **3**, 4780.
3 M. Kaur, J. S. McCloy, W. Jian, Q. Yao and Y. Qiang, *J. Phys. Chem. C*, 2012, **116**, 12875.
4 C. Xu, D. Ho, J. Xie, C. Wang, N. Kohler, E. G. Walsh, J. R. Morgan, Y. E. Chin and S. Sun, *Angew. Chem., Int. Ed.*, 2008, **47**, 173.
5 A. J. Mieszawska, R. Jalilian, G. U. Sumanasekera and F. P. Zamborini, *Small*, 2007, **3**, 72 and references therein.
6 C. Langlois, Z. L. Li, J. Yuan, D. Alloyeau, J. Nelayah, D. Bochicchio, R. Ferrando and C. Ricolleau, *Nanoscale*, 2012, **4**, 3381.
7 G. A. Sotiriou, *WIREs Nanomed. Nanobiotechnol.*, 2013, **5**, 19–30.
8 Z. Fan, M. Shelton, A. K. Singh, D. Senapati, A. S. Khan and P. C. Ray, *ACS Nano*, 2012, **6**, 1065.
9 C. Wang, J. Chen, T. Talavage and J. Irudayaraj, *Angew. Chem., Int. Ed. Engl.*, 2009, **48**, 2759.
10 X. Ji, R. Shao, M. A. Elliott, J. R. Stafford, E. Esparza-Coss, A. J. Bankson, G. Liang, P. Z. Luo, K. Park, T. J. Markert and C. Li, *J. Phys. Chem. C*, 2007, **111**, 6245.
11 H. Ido and T. Itoh, *Electronic structure and Magnetism of 3d-Transition Metal Pnictides*, Springer, 2009.
12 M. Hansen, *Constitution of Binary Alloys*, Geminuim Publ. Co., New York, 1985, p. 502.
13 X. H. Liu, N. Zhang, R. Yi, G. Z. Qiu, A. G. Yan, H. Y. Wu, D. P. Meng and M. T. Tang, *Mater. Sci. Eng., B*, 2007, **140**, 38.
14 J. H. Zhang, X. G. Yang, S. D. Li, Y. Xie, W. C. Yu and Y. Qian, *J. Solid State Chem.*, 2000, **152**, 537.
15 J. F. Zhao, J. M. Song, C. C. Liu, B. H. Liu, H. L. Niu, C. J. Mao, S. Y. Zhang, Y. H. Shen and Z. P. Zhang, *CrystEngComm*, 2011, **13**, 5681.
16 L. Zhang and C. Zhang, *Nanoscale*, 2014, **6**, 1782–1789.

17 F. Liu, B. Wang, Y. Lai, J. Li, Z. Zhang and Y. Liu, *J. Electrochem. Soc.*, 2010, **157**, D523.
18 N. Umeyama, M. Tokumoto, S. Yagi, M. Tomura, K. Tokiwa, T. Fujii, R. Toda, N. Miyakawa and S. Ikeda, *Jpn. J. Appl. Phys.*, 2012, **51**, 053001.
19 C. E. M. Camposa, J. C. de Limaa, T. A. Grandia, K. D. Machadoa and P. S. Pizanib, *Phys. B*, 2002, **324**, 409.
20 C. Wang, C. Xu, H. Zeng and S. Sun, *Adv. Mater.*, 2009, **21**, 3045.
21 Y. Jin, C. Jia, S. Huang, M. O'Donnell and X. Gao, *Nat. Commun.*, 2010, **1**, 1.
22 X. Liu, N. Zhang, R. Yi, G. Qiu, A. Yan, H. Wu, D. Meng and M. Tang, *Mater. Sci. Eng., B*, 2007, **140**, 38.
23 H. Okamoto and T. B. Massalski, *Bull. Alloy Phase Diagrams*, 1985, **6**, 229.
24 A. B. Mandale, S. Badrinarayanan, S. K. Date and A. P. B. Sinha, *J. Electron Spectrosc. Relat. Phenom.*, 1984, **33**, 61.
25 M. Hu, J. Chen, Z. Li, L. Au, G. V. Hartland, X. Li, M. Marqueze and Y. Xia, *Chem. Soc. Rev.*, 2006, **35**, 1084.
26 C. Shen, C. Hui, T. Yang, C. Xiao, J. Tian, L. Bao, S. Chen, H. Ding and H. Gao, *Chem. Mater.*, 2008, **20**, 6939.
27 E. P. Tijerina, M. Garcia Pinilla, S. Mejia-Rosales, U. Oritz-Mendez, A. Torres and M. Jose-Yacaman, *Faraday Discuss.*, 2008, **138**, 353.
28 D. P. Mills, F. Moro, J. McMaster, J. Slageren, W. Lewis, A. J. Blake and S. T. Liddle, *Nat. Chem.*, 2011, **3**, 454.
29 R. H. Kodama, C. L. Seaman, A. E. Berkowitz and B. Mapple, *J. Appl. Phys.*, 1994, **75**, 5639.
30 S. Mishra, K. Song, J. A. Koza and M. Nath, *ACS Nano*, 2013, **7**, 1145.
31 S. Mishra, K. Song, K. Ghosh and M. Nath, *ACS Nano*, 2014, **8**, 2077.